



Impact of temperature and water availability on microwave-derived gross primary production

Irene E. Teubner^{1,2}, Matthias Forkel³, Benjamin Wild¹, Leander Mössinger¹, and Wouter A. Dorigo¹

¹Department of Geodesy and Geoinformation, TU Wien, Wiedner Hauptstraße 8, 1040 Vienna, Austria

²Zentralanstalt für Meteorologie und Geodynamik (ZAMG), Hohe Warte 38, 1190 Vienna, Austria

³Environmental Remote Sensing Group, Institute of Photogrammetry and Remote Sensing, Technische Universität Dresden, Helmholtzstraße 10, 01069 Dresden, Germany

Correspondence: Irene E. Teubner (irene.teubner@zamg.ac.at)

Abstract. Vegetation optical depth (VOD) from microwave satellite observations has received much attention in global vegetation studies in recent years due to its relationship to vegetation water content and biomass. We recently have shown that VOD is related to plant productivity, i.e. gross primary production (GPP). Based on this relationship between VOD and GPP we developed a theory-based machine learning model to estimate global patterns of GPP from passive microwave VOD retrievals. The VOD-GPP model generally showed good agreement with site observations and other global data sets in temporal dynamic but tended to overestimate annual GPP across all latitudes. We hypothesized that the reason for the overestimation is the missing effect of temperature on autotrophic respiration in the theory-based machine learning model. Here we aim to further assess and enhance the robustness of the VOD-GPP model by including the effect of temperature on autotrophic respiration within the machine learning approach and by assessing the interannual variability of the model results with respect to water availability. We used X-band VOD from the VOD Climate Archive (VODCA) data set for estimating GPP and used global state-of-the-art GPP data sets from FLUXCOM and MODIS to assess residuals of the VOD-GPP model with respect to drought conditions as quantified by the Standardized Precipitation and Evaporation Index (SPEI).

Our results reveal an improvement in model performance for correlation when including the temperature dependency of autotrophic respiration. This increase in temporal dynamic is largest for regions outside the tropics. For error and bias, the results are regionally diverse and are compensated in the global average. On interannual time scales, estimates of the VOD-GPP model agree well with GPP from FLUXCOM and MODIS. We further find that the residuals between VOD-based GPP estimates and the other data sets do not significantly correlate with SPEI which demonstrates that the VOD-GPP model can capture responses of GPP to water availability even without including additional information on precipitation, soil moisture or evapotranspiration. However, some regions reveal significant correlations between VOD-GPP residuals with SPEI, which may indicate different plant strategies for dealing with variations in water availability.

Overall, our findings support the robustness of global microwave-derived estimates of gross primary production for large-scale studies on climate-vegetation interactions.



1 Introduction

25 Vegetation optical depth (VOD) from microwave satellite observations provide the opportunity for studying large-scale vegeta-
tion dynamics due to its sensitivity to the vegetation water content and above-ground biomass. Different studies have employed
VOD for deriving various plant properties or vegetation characteristics that can be related to the plant's water content, includ-
ing biomass estimation (Liu et al., 2015), crop yield (Chaparro et al., 2019), tree mortality (Rao et al., 2019; Sapes et al.,
2019), analysis of burned area (Forkel et al., 2019) and ecosystem-scale isohydrlicity (Konings and Gentine, 2017). VOD, or
30 microwave satellite observations in general, are also analyzed for its potential in detecting the impact of drought (Song et al.,
2019; Crocetti et al., 2020). Despite the sensitivity of VOD to vegetation water content, the relationship between VOD and
GPP has not yet been analyzed with regard to whether it holds true along a gradient of dry- or wetness conditions.

Recently, we have shown that VOD is related to plant productivity, i.e. gross primary production (GPP) (Teubner et al., 2018).
Based on these findings, we developed a theory-guided machine learning model to estimate GPP from VOD (VOD-GPP model)
35 and trained the model using eddy covariance estimates of GPP from the FLUXNET network (Teubner et al., 2019). The VOD-
GPP model relies on estimating carbon sink terms, i.e. net primary production (NPP) and autotrophic respiration (Ra), based
on VOD as a proxy for aboveground living biomass. The VOD-GPP model thus represents a carbon sink-driven approach. Due
to the utilization of biomass as main input to the VOD-GPP model, the estimation does not rely on input variables that are
commonly used in source-driven approaches, e.g. absorption of photosynthetically active radiation as primary input term or
40 vapor pressure deficit as controlling factor for stomatal conductance (Running et al., 2000; Turner et al., 2005; Goodrich et al.,
2015; Zhang et al., 2016, 2017). Although different studies are tackling the question of how much information on biomass is
actually contained in the VOD signal (Momen et al., 2017; Vreugdenhil et al., 2018; Zhang et al., 2019), it might be worth
noting that the water content can be seen as a necessity for our model, since only living cells that contain water are able to
respire. We have shown that the VOD-GPP model can well represent temporal dynamics of GPP but that it overestimates GPP
45 especially in temperate and boreal regions (Teubner et al., 2019). We hypothesize that this overestimation may be caused by a
missing representation of temperature dependency of autotrophic respiration in the VOD-GPP model.

Ra is the process through which chemical energy that was stored by building up carbohydrates during photosynthesis is
gained by converting carbohydrates back into carbon dioxide. It is generally known that Ra is a temperature-dependent process
(e.g., Atkin and Tjoelker, 2003). Modelling the response of Ra to temperature, however, is complex due to the existence of
50 thermal acclimation (Atkin and Tjoelker, 2003). Ra is commonly represented through an exponential function with Q10 as
base which is multiplied with a basal respiration rate (e.g., Smith and Dukes, 2013). The base value Q10 describes how much
Ra changes when temperature changes by 10°C (e.g., Atkin et al., 2008). Although global models often use constant values for
either one parameter or both parameters (Gifford, 2003; Smith and Dukes, 2013), studies have shown that both basal respiration
rate and Q10 may vary with temperature (Tjoelker et al., 2001; Wythers et al., 2013). The implementation of such temperature
55 acclimation yields a functional representation that decreases again at higher temperatures and thus takes into account that
respiration may decrease outside an optimum temperature range (Smith and Dukes, 2013).



Here we aim to assess the impact of the temperature dependency of R_a in the VOD-GPP model and if it can improve model performance. Furthermore, we will test the plausibility of the model by comparing the estimated interannual variability of GPP with independent state-of-the-art global data sets of GPP and by assessing model residuals with respect to variations in climatological water availability as represented by the Standardized Precipitation and Evaporation Index (SPEI). Since source- (GPP) and sink-terms ($NPP + R_a$) should theoretically be in balance, any differences between the two approaches that are related to variations in water availability may give insight into different plant strategies for dealing with dry or wet conditions and thus may be of interest for ecological or plant-physiological studies at large-scale.

2 Data and methods

We analysed different GPP data sets derived from microwave and optical sensors as well as SPEI. As input to the VOD-GPP model we used X-band VOD data from the VOD Climate Archive (VODCA). Since global coverage for VODCA data starts in 2003 (Moesinger et al., 2020) and SPEI data are available through 2015, we used the common period from 2003 to 2015 for our analysis. Temporal median maps for the global GPP data sets are displayed in the supplement (Figure A1).

2.0.1 VODCA

VOD from microwave satellite observations often spans only a few years, which thus prevents the analysis of longer periods. To overcome this problem, we used a merged single frequency VOD from the VOD Climate Archive (VODCA; Moesinger et al., 2020) as input to our model. Since previous analysis revealed that X-band VOD shows the closest agreement with GPP, both for the direct comparison between VOD and GPP (Teubner et al., 2018, 2019) as well as for the assimilation in land surface models (Kumar et al., 2020), we used VODCA X-band VOD to estimate GPP. VODCA (Moesinger et al., 2020) X-band (VODCAX) contains passive VOD derived from TMI (10.7 GHz), AMSR-E (10.7 GHz), WindSat (10.7 GHz) and AMSR2 (10.7 GHz). The VOD input data are obtained from the Land Parameter Retrieval Model (LPRM; van der Schalie et al., 2017). VODCAX is derived from nighttime observations from TMI (variable overpass time), AMSR-E (descending 1:30 am), WindSat (descending 6:00 am) and AMSR2 (descending 1:30 am). The use of nighttime observations on the one hand meets the LPRM assumption of homogeneous temperature conditions and on the other hand is better suited as proxy for plant water status than daytime observations. Due to diurnal differences in plant water status and the refilling during the night (El Hajj et al., 2019; Konings and Gentine, 2017), nighttime observations are closer to the predawn water potential which is commonly used as estimator for the daily vegetation water status (Konings and Gentine, 2017; Konings et al., 2019). During data processing, data were masked for radio frequency interference (RFI) since RFI can introduce spurious retrievals (Li et al., 2004; Njoku et al., 2005). Data are available at daily resolution and 0.25° grid spacing.

2.0.2 Independent global GPP data sets

The MOD17A2H v006 product provides global estimates of GPP which are derived from surface reflectances (Running et al., 2004, 2015). The algorithm is based on the light-use efficiency concept by Monteith (1972) and uses the fraction of Photosyn-



thetically Absorbed Radiation for deriving plant productivity (Running et al., 1999, 2000). Data are produced as 8-daily GPP estimates at 500 m resolution.

90 FLUXCOM presents an upscaling of GPP from eddy covariance measurements using an ensemble of machine learning approaches (Jung et al., 2020). The data set is available at 8-daily resolution and 10 km grid spacing. FLUXCOM estimates are produced in two setups: the FLUXCOM RS is based on remote sensing data as input to the machine learning models and the FLUXCOM RS+METEO uses meteorological data and only the mean seasonal cycle of remote sensing data (Jung et al., 2020). Since our approach is mainly based on remote sensing data, we used FLUXCOM RS in our analysis. The FLUXCOM
95 algorithm uses the following MODIS variables as input: Enhanced Vegetation Index, Leaf Area Index, MODIS band 7 - Middle Infrared Reflectance, Normalized Difference Vegetation Index and Normalized Difference Water Index.

2.0.3 In situ GPP estimation from FLUXNET

The Fluxnet2015 data set (Gilberto et al., 2020) provides daily in situ estimates of carbon, water and heat fluxes, which are determined using the eddy covariance technique. GPP estimates are available for two flux partitioning methods, i.e. daytime
100 and nighttime partitioning method. We used the mean of both partitioning methods, as suggested in (Gilberto et al., 2020), with variable friction velocity threshold (GPP_DT_VUT_REF, GPP_NT_VUT_REF) from the freely available station data set (Tier1 v1). Since data are available until 2014, we used data for the period from 2003 to 2014 as training data for estimating GPP based on VOD. An overview of the FLUXNET sites is given in Figure A2 and Table A1.

2.0.4 SPEI

105 For analyzing the impact of variations in water availability, we used SPEI from the SPEIbase (Beguería et al., 2017; Vicente-Serrano et al., 2010). The climatological water balance is calculated on different time scales ranging from 1 up to 48 months. Since drought can act on different time scales, we used SPEI at two different aggregations, 3- and 12-month, for investigating the response to dry and wet conditions. The 3-month SPEI (SPEI03) represents short-term effects, while the 12-month SPEI (SPEI12) relates to dry or wet conditions at annual time scale. Although SPEI cannot be used to express actual water shortage
110 for plants, it allows to indicate relative deviations from mean conditions. Because of the use of both precipitation and temperature, SPEI further enables the comparison between different biomes (Vicente-Serrano et al., 2010). The SPEI data has monthly resolution and a grid spacing of 0.5°.

2.0.5 ERA5-Land

ERA5-Land produced by the European Centre for Medium-Range Weather Forecasts (ECMWF) (C3S, 2019; Muñoz-Sabater,
115 2019) provides a reanalysis data set of meteorological parameters. ERA5 uses a 4D variational data assimilation scheme and a Simplified Extended Kalman Filter (Hersbach et al., 2020). We used skin temperature and snow data for masking VOD. In the VOD-GPP model, we incorporated 2m air temperature (T2M) for representing the temperature dependency of autotrophic



respiration. T2M was used in our analysis, since this parameter is most common for describing the temperature dependency of autotrophic respiration for aboveground vegetation. The data has hourly resolution and 9 km spatial sampling.

120 2.1 Data processing

VODCAX data were masked for low temperature (skin temperature $< 0^{\circ}\text{C}$) and snow cover (snow depth $> 0\text{cm}$) and aggregated to 8-daily estimates by computing the mean over 8 days. These 8-daily values were then used as input to the VOD-GPP model. GPPfluxcom and GPPmodis were aggregated to 0.25° to match the spatial sampling of VODCAX. For the comparison with SPEI, GPP estimates were further resampled to monthly resolution while SPEI was spatially resampled to 0.25° using the
125 nearest neighbour method.

2.2 GPP estimation based on VOD

The approach of estimating GPP based on microwave radiation is described in detail in Teubner et al. (2019). In short, the VOD-GPP model uses VOD as a proxy for aboveground living biomass and determines GPP by estimating sinks for carbohydrates, i.e. the sum of NPP and R_a , which are represented through different VOD variables: VOD time series, temporal change in
130 VOD (ΔVOD) and the grid cell median of VOD (mdnVOD; as a proxy for vegetation cover). While NPP is related to ΔVOD , R_a is related to both VOD and ΔVOD using the concept by Ryan et al. (1997) of dividing R_a into maintenance and growth respiration. This previous model formulation, which uses only VOD variables as input (GPPvod; Equation 1), thus reads:

$$\text{GPPvod} = s(\text{VOD}) + s(\Delta\text{VOD}) + s(\text{mdnVOD}) \quad (1)$$

where s denotes spline terms for representing the 2-dimensional functions between each input variable and the response
135 variable GPP.

For adding the temperature dependency of R_a , we are considering the two terms of R_a , i.e. maintenance and growth respiration. Since the temperature sensitivity mainly applies to the maintenance term (Ryan et al., 1997), we are only incorporating an interaction term with temperature for the maintenance part of the model formulation. Although all terms potentially may be dependent on temperature due to the general temperature dependency of enzymatic activity, the temperature dependency
140 for modelling growth related sink terms (growth respiration and net primary production) may be of less importance. For the current model formulation (GPPvodtemp; Equation 2), we now introduced an interaction term between VOD and temperature:

$$\text{GPPvodtemp} = te(\text{VOD}, T2M) + s(\Delta\text{VOD}) + s(\text{mdnVOD}) \quad (2)$$

where te stands for a tensor term, which represents the interaction between VOD and temperature and spans a 3-dimensional surface.

145 Consistent with our previous model, we used GAM as regression method for deriving GPP. pyGAM (Servén and Brummitt, 2018) version 0.8.0 provides the possibility of adding an interaction term. An advantage of GAM is that the relationships



between input variables and response variable are not required to be known beforehand, but instead can be estimated from the data itself (Hastie and Tibshirani, 1987). Since the relationship between VOD and GPP as well as its relationship with temperature is difficult to determine a priori, this method is well suited for our approach.

150 The model was fitted using a smoothing factor of 2, which is lower than for the previous model. This was done since the response function for the tensor term was too smooth using the default number of 10 splines for tensor terms and resulted in unrealistically high GPP values at high VOD. For Δ VOD, the default number of 20 splines for spline terms were used, while for mdnVOD we reduced the number of splines to 5 in order to obtain a smooth relationship.

2.3 Statistical analysis

155 For model comparison, we computed Pearson correlation, unbiased Root Mean Square Error (ubRMSE) and bias. For studying the error characteristics, ubRMSE was used instead of RMSE to exclude the impact of bias, which was observed during our analysis.

In case of analyzing annual GPP anomalies as a measure for interannual variability and residuals of the VOD-GPP model, we based our analysis on standardized annual or 8-daily time series data (z-scores). This was done in order to analyze GPP data in the absence of systematic differences between the data sets. The standardization for the 8-daily or the annual data was applied to each grid cell time series by subtracting the mean and dividing by the standard deviation.

160

For aid visual comparison in the time series plots, we applied a savitzky-golay filter with window size of 11 data points.

3 Results

3.1 Model representation of temperature dependency

165 We find that the sensitivity of VOD to GPP increases with temperature as shown by the partial dependency plots (Figure 1). For low temperatures, the sensitivity of the VOD-GPP-relationship is relatively low (Figure 1a). As temperature increases, the sensitivity also increases and further exhibits an optimum behavior. At high temperatures, however, the maxima of the curves are lower than for moderate temperatures. The partial dependency for T2M (Figure 1d) shows an optimum behavior with a peak around 20°C, which slightly differs between the VOD values. The partial dependencies for Δ VOD and mdnVOD (Figure 1b,c) are consistent the previous model and yield a positive relationship with GPP for Δ VOD in the middle part of the value range and a general decreasing relationship for mdnVOD.

170

In addition to identifying the underlying relationships, we can further assess the magnitude of the contribution to GPP for the input variables based on the data range in the partial dependency plots. The main contribution to GPP in the model comes from the interaction term between VOD and T2M with a range of about 12 gC m⁻² d⁻¹, which is followed by Δ VOD with a range of about 6 gC m⁻² d⁻¹ and mdnVOD with a range of about 4 gC m⁻² d⁻¹. The contribution of the maintenance part, as represented through the interaction term, thus, is higher than for Δ VOD which represents the sum of NPP and the growth term in Ra.

175

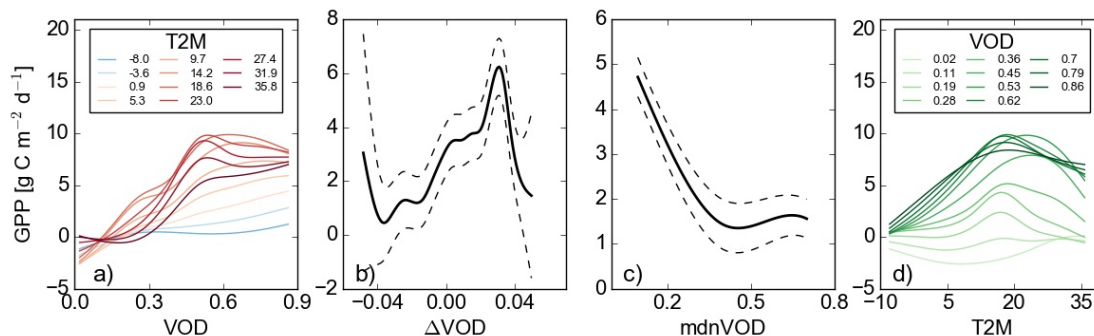


Figure 1. Partial dependency plot for GPPvotemp. The interaction between VOD and T2M, which represents a 3D surface, is displayed as projection on the 2D plane for each of the two input variables. For this, the parameter space was divided into 10 equally spaced bins between minimum and maximum of the respective variable.

3.2 Evaluation at site-level

At FLUXNET in situ stations, GPPvotemp, GPPfluxcom and GPPmodis overall show similar results (Figure 2). Despite the
180 overall agreement with in situ GPP, all three data sets exhibit an underestimation of GPP at high values of GPP compared with
in situ GPPfluxnet. At annual time scale, the difference with GPPfluxnet at high GPP becomes much lower for GPPvotemp
compared to GPPfluxcom and GPPmodis (Figure A3), which indicates on the one hand that GPPvotemp is able to match the
in situ training data and on the other hand suggests that differences in GPP already exist between the training data set used
in our study and the independent global GPP data sets, which may contribute to differences at global scale. At low in situ
185 GPP, we observe that GPPvotemp tends to overestimate GPP compared to the other data sets, which can also be observed
at annual time scale. This overestimation at low GPP may be an explanation for the general tendency for overestimation of
microwave-derived GPP estimates and appears to not be related to the temperature sensitivity of Ra.

3.3 Impact of adding temperature dependency at the global scale

Performance metrics for GPPvod and GPPvotemp were assessed with respect to both GPPfluxcom and GPPmodis. Since the
190 results for GPPfluxcom and GPPmodis are similar, we are only showing results for GPPfluxcom.

Correlations with GPPfluxcom (Figure 3a) reveal widespread strongly positive values with a global mean of 0.63. Some areas
in the tropics and in the Australian desert exhibit an inverse temporal dynamic with GPPfluxcom. Compared with GPPvod,
correlations increase in large parts of the world (Figure 3b) with a global average difference of 0.18. Regions that benefit most
from adding temperature as input are temperate and cold regions, which could be expected since these regions per definition are
195 strongly controlled by temperature. Tropics and subtropics, however, mainly show only minor changes in correlation coefficient
with a few exceptions of decreasing correlations. Since the annual temperature amplitude in these regions is low, the model's
sensitivity to temperature is also low, which makes the interaction term mainly controlled by VOD.

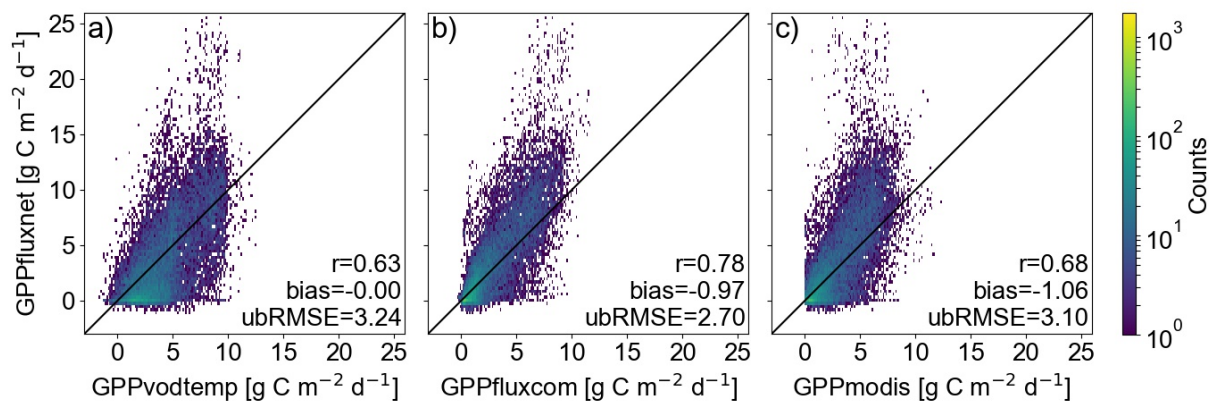


Figure 2. Scatter plots of 8-daily in situ GPPfluxnet versus global GPP data sets GPPvodtemp, GPPfluxcom and GPPmodis.

The global average for ubRMSE between GPPvodtemp and GPPfluxcom (Figure 3c) yields a value of 1.20. Consistent with the increase in performance for the correlation, areas in the temperate and cold region show an improvement in error, i.e. a decrease of ubRMSE compared to GPPvod (Figure 3d). Other regions, however, exhibit an increase in ubRMSE. The global average of the difference between results for GPPvodtemp and GPPvod is -0.05. Therefore, gains and losses in error are largely compensated at the global scale.

The bias between GPPvodtemp and GPPfluxcom (Figure 3c) is generally positive everywhere with a global average of 1.64. This finding is also evident from the higher range in the median maps for GPPvodtemp compared with GPPfluxcom and GPPmodis (Figure A1). Comparing the results for GPPvod and GPPvodtemp, the addition of temperature shows an increase in bias mainly in the tropics (Figure 3d). Despite this increase in the tropics, also regions with a reduction in bias exist, which are mainly found in temperate and cold regions. On the global scale, decreases and increases in bias compensate and yield an average difference of -0.05.

The latitudinal distribution of annual GPP (Figure 4) further demonstrates that the addition of temperature yields a reduction of GPP mainly for regions outside -35°N and $+60^{\circ}\text{N}$. The reduction in the zonal mean, however, is smaller than may have been expected probably due to compensating effects. For the region between $+30^{\circ}\text{N}$ and $+60^{\circ}\text{N}$, where reductions in bias were observed on the global map, positive and negative values for the bias appear to compensate yielding no net reduction in the zonal mean. In the tropical region, the increase in bias for GPPvodtemp compared with GPPvod is again evident. When considering the latitudinal distribution of annual GPP relative to the latitudinal maximum, however, the distribution for GPPvodtemp is actually closer to the independent datasets than GPPvod (Figure A4). This suggests that although the bias largely increases in the tropics, the relative distribution between tropics and temperate to boreal regions is better represented by the setup that includes temperature.

For a region in Europe, where we generally did observe an increase all three performance metrics, we find that for GPPvod mainly winter time estimates of GPP are too high compared to GPPfluxcom and GPPmodis (Figure 5). By adding temperature

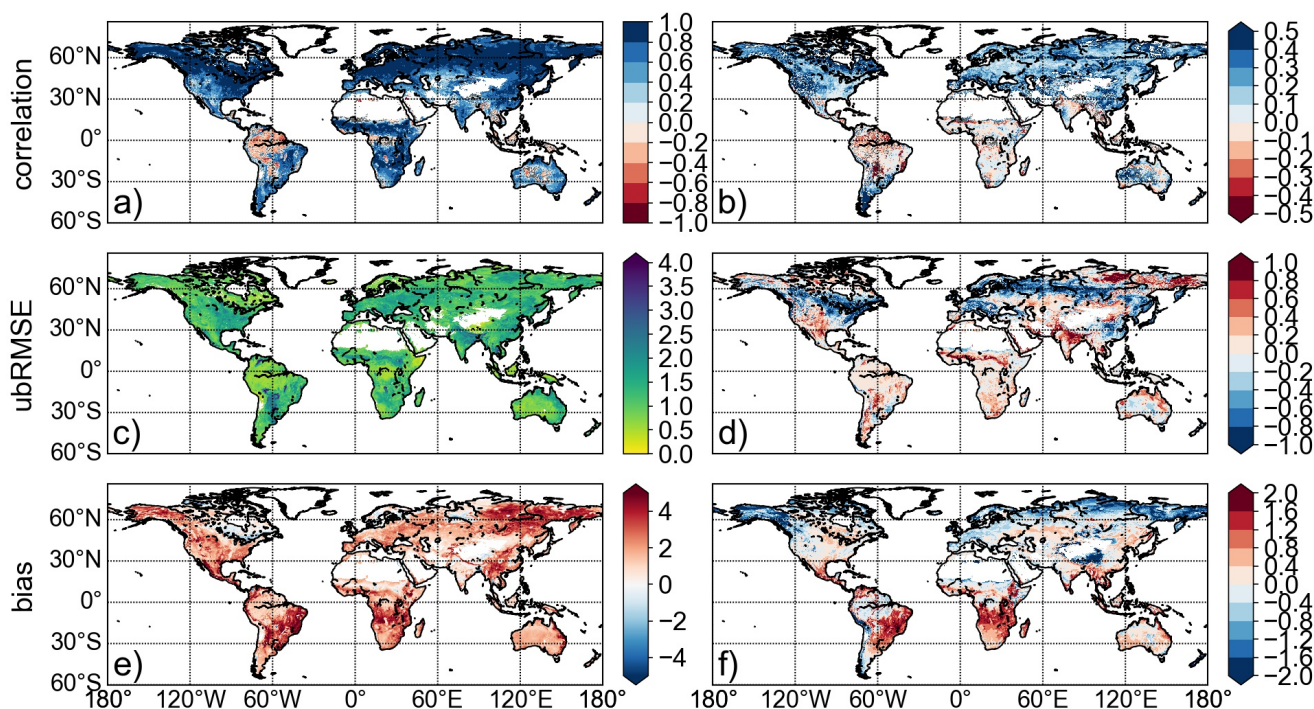


Figure 3. (a): Pearson correlation between GPPvodtemp and GPPfluxcom. (b): Difference between GPPvodtemp and GPPvod for Pearson correlation with GPPfluxcom. (c): ubRMSE between GPPvodtemp and GPPfluxcom. (d): Difference between GPPvodtemp and GPPvod for ubRMSE with GPPfluxcom. (e): Bias between GPPvodtemp and GPPfluxcom. (f): Difference between GPPvodtemp and GPPvod for the bias with GPPfluxcom. The unit for ubRMSE and bias is $\text{g C m}^{-2} \text{d}^{-1}$. Areas with none significant correlations in (a) and (b) are marked in grey.

220 as input to the model, winter observations are markedly dampened and summer observations are only slightly increased. Nevertheless, even when including the temperature dependency, winter GPP estimates are still slightly higher for GPPvodtemp than for GPPfluxcom or GPPmodis.

Due to the observed bias (both at site-level and global scale), but otherwise increase in correlation, we are further analyzing GPPvodtemp but are focusing on relative rather than absolute values for comparing interannual variability and the impact of
225 water availability in the remaining study.

3.4 Interannual variability and varying conditions of water availability

The latitudinal distribution of annual GPP anomalies reveals a general agreement between the GPP data set (Figure 6). Although differences exist between all data sets, key features such as the positive anomalies at -55°N in 2003, at -30°N in 2011 or at

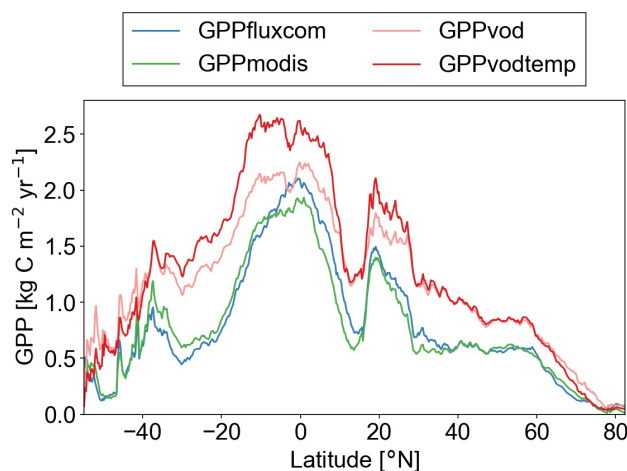


Figure 4. Zonal mean of annual GPP for GPPfluxcom, GPPmodis, GPPvodtemp and GPPvod.

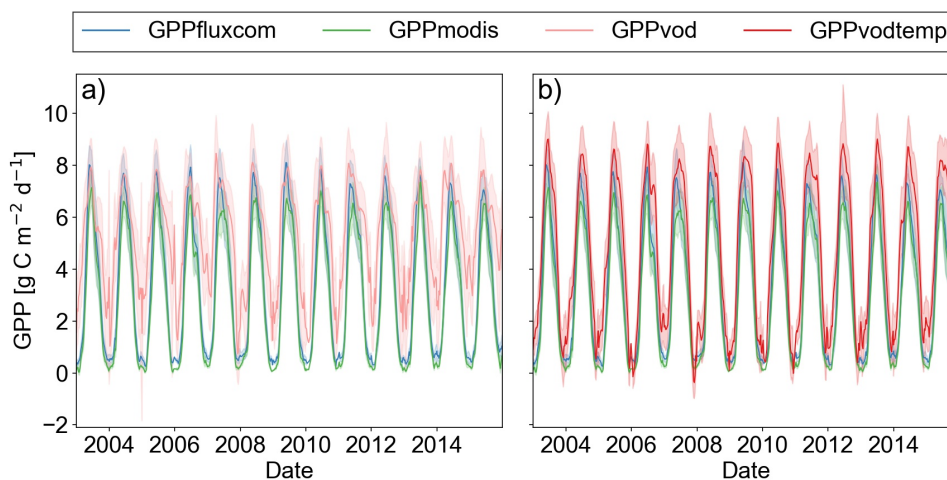


Figure 5. Time series plot of spatially aggregated GPP estimates for GPPfluxcom, GPPmodis and a) GPPvod or b) GPPvodtemp. Shaded areas indicate the standard deviation over the aggregated grid cells. The region is located in Europe, 5 to 15°E and 46 to 51°N. 8-daily data were smoothed to aid visual comparison.

+75°N in 2012 and the negative anomalies at +75°N in 2003 and 2015 and at around -40° in 2009 and 2011. Despite the fact
230 that these key features are found in all data sets, we also observe that the magnitude of the anomalies often differs between
the data sets, which thus yields a generally relatively high variability between all data sets. In terms of the overall latitudinal
pattern, it appears that GPPvodtemp is more similar to GPPmodis than to GPPfluxcom.

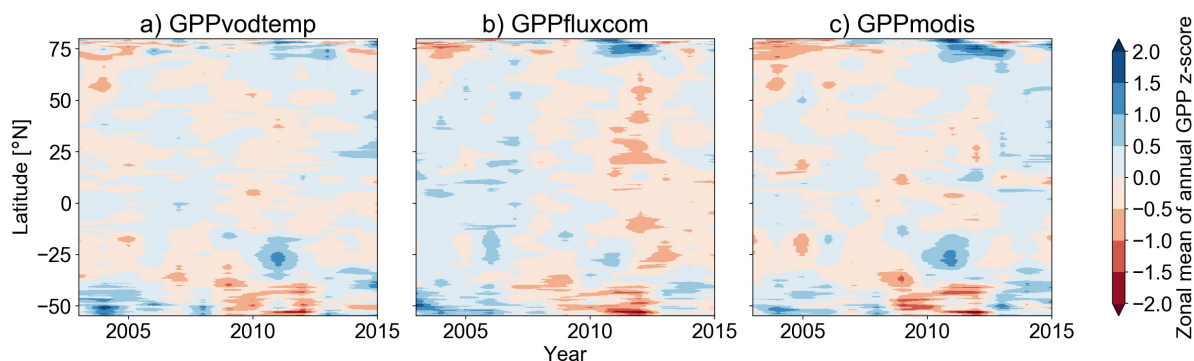


Figure 6. Hovmöller diagramm for zonal means of annual GPP anomalies (z-scores) for GPPvodtemp, GPPfluxcom and GPPmodis.

For the correlation of the residuals between standardized GPP (GPPvodtemp-GPPfluxcom or GPPvodtemp-GPPmodis) with SPEI, we find that large areas show no significant correlation with SPEI03 (Figure 7a,b). For the long-term climatological water balance, i.e. SPEI12 (Figure 7c,d), these areas with none significant correlations further increase. In terms of model applicability, the none significant correlations are the desired result. Given that correlations in these regions are high, this demonstrates that GPPvodtemp shows a similar behavior as GPPfluxcom or GPPmodis in response to variations in dry or wet conditions, which further indicates that the VOD-GPP-relationship in general holds true.

Apart from the widespread areas with none significant correlation, some significant correlations, both positive and negative, occur at both time scales. Negative correlations indicate that during dry conditions GPPvodtemp is higher relative to the reference GPP than during wet conditions, while positive correlations mean that during dry conditions GPPvodtemp is lower relative to the reference GPP than during wet conditions. The spatial distribution of these significant correlations is largely consistent between GPPfluxcom and GPPmodis. For the short-term response to SPEI (Figure 7a,b), negative correlations are more frequent than positive correlations, indicating that the response to short-term drought events is often a reduction of source-driven GPP relative to sink-driven GPP. Negative correlations are mainly observed in the US corn belt, Argentina, Eastern Europe, Russia and China, with the strongest negative correlations being in the US, Argentina and Russia. Positive correlations are obtained mainly over South America, Africa and Australia. For the long-term response to SPEI (Figure 7c,d), the number of positive correlations increase. Similar to the short-term response, positive correlations are mainly found over South America, Africa and Australia.

For specific regions, which are indicated in Figure 7, we analyzed the time series of the standardized GPP (Figure 8) and the response to SPEI categories (Figure A5) in order to inspect under which situations negative or positive correlations with SPEI occur.

For the region in the US corn belt (Figure 8a), where we found moderately negative correlations with SPEI, all three GPP data sets show a reduction in summer GPP in 2006 and 2012. Compared with other years, however, the reduction of GPPvodtemp tends to be less than for GPPfluxcom and GPPmodis. This behavior can be verified by considering the residuals along the SPEI12 gradient (Figure A5a). During dry conditions, the residuals are higher than during wet conditions. Since

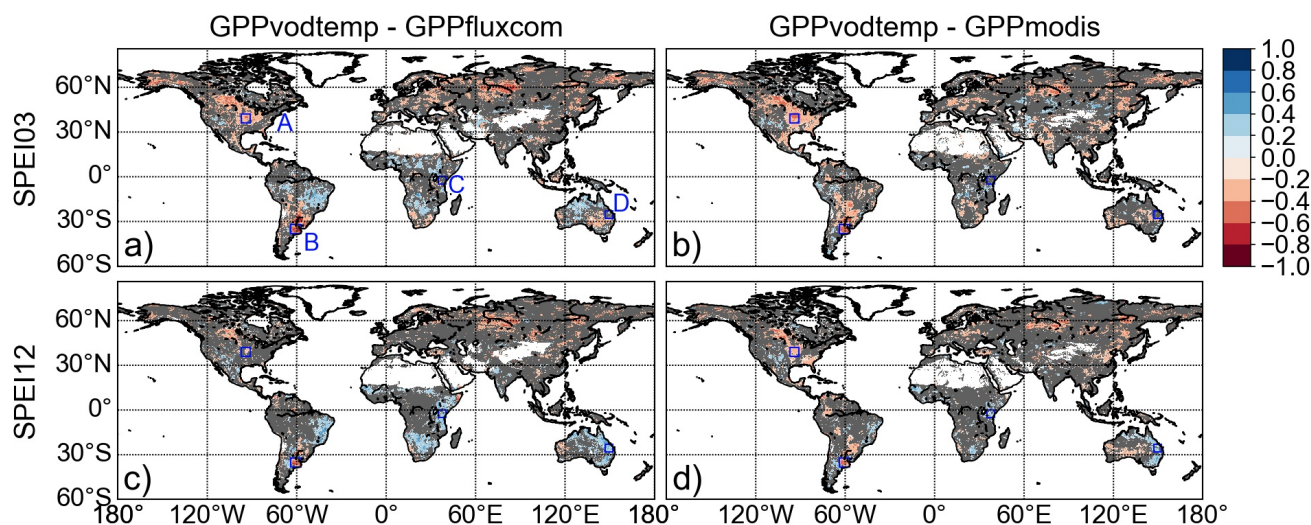


Figure 7. Correlation between residuals of standardized GPP ($GPP_{vodtemp} - GPP_{fluxcom}$ and $GPP_{vodtemp} - GPP_{modis}$) and SPEI. None significant correlations are indicated in grey. (a,c): $GPP_{vodtemp} - GPP_{fluxcom}$, (b,d): $GPP_{vodtemp} - GPP_{modis}$, (a,b): SPEI03 (short-term response), (c,d): SPEI12 (long-term response). Regions A-D: US cornbelt (A), Argentina (B), Eastern Africa (C) and Eastern Australia (D).

higher residuals indicate that $GPP_{vodtemp}$ is higher relative to the reference data sets, this result confirms the findings for the time series.

In Argentina (Figure 8b), we observed strongly negative correlations for the analysis with SPEI. For this region, a pronounced
260 dry condition is observed at the end of 2008 and beginning of 2009. In this period, $GPP_{fluxcom}$ and GPP_{modis} are reduced
more strongly than $GPP_{vodtemp}$. In the first following year, the $GPP_{vodtemp}$ peak is slightly lower than for $GPP_{fluxcom}$
and GPP_{modis} at the end of 2009. In the second following year, end of 2011, $GPP_{vodtemp}$ is similar as for $GPP_{fluxcom}$ and
 GPP_{modis} again. This result is further supported by the pronounced decrease of the residuals with SPEI12 in Figure 8b. In
addition to the interannual variability, we also find that the spring peak is more pronounced in $GPP_{fluxcom}$ and GPP_{modis} than
265 in $GPP_{vodtemp}$, which might point towards a surplus of carbohydrates in spring that are incorporated for building up biomass
later in the year or may be related to differences in land cover.

For the example in Africa (Figure 8c), where correlations with SPEI12 were positive, $GPP_{vodtemp}$ generally appears to
be a bit higher relative to $GPP_{fluxcom}$ and GPP_{modis} at the end of each growing period. In face of dry conditions, however,
 $GPP_{vodtemp}$ shows a stronger reduction in GPP than $GPP_{fluxcom}$ and GPP_{modis} at the end of the growing season, as observed
270 in 2006 and 2009. Despite some differences in the time series between $GPP_{vodtemp}$ and the reference data sets, the temporal
dynamic is generally similar between the data sets. This indicates that the sink-driven GPP shows a slightly different response
to changes in environmental conditions for this region, which then results in the observed positive correlations with SPEI.

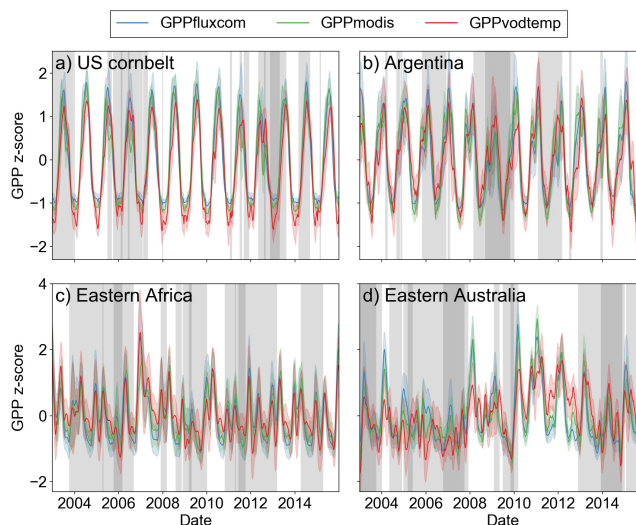


Figure 8. Regional mean of standardized GPP values for regions as indicated in Figure 7. Shaded areas denote the standard deviation for the regional aggregated time series. Vertical grey areas indicate periods with different levels of dryness conditions for regional aggregated SPEI12: $SPEI12 < -1$ (dark grey), $-1 \leq SPEI12 < 0$ (light grey) and $SPEI12 \geq 0$ (white areas). Data were smoothed to aid visual comparison.

Considering the residuals along the SPEI12 gradient for this region, we find that the residuals increase with SPEI12 for all categories except for very wet conditions (Figure A5c).

275 The time series for Australia (Figure 8d) shows that GPPvodtemp is generally reduced during dry conditions and increases relative to GPPfluxcom and GPPmodis during wet conditions. The increase in GPPvodtemp relative to the reference data sets appears to be strongest for the period following one year after long-term dry conditions, i.e. in 2009, 2011 and 2012. Consistently, the residuals show a clear increase along the SPEI12 categories (Figure A5d).

4 Discussion

280 4.1 Impact of adding temperature as model input

The performance of the VOD-GPP model was shown to improve with the addition of an interaction term between VOD and temperature mainly in terms of temporal dynamic. Our results showed that the increase in temporal dynamic was mainly observed for temperate and cold regions. Since the growing season in these regions is largely controlled by temperature, this indicates that the improvement may largely be a seasonal effect. When analyzing the temperature response of respiration across
285 biomes, both spatial and temporal differences resulting from thermal acclimation need to be taken into account (Vanderwel et al., 2015). On the spatial scale, temperature sensitivity largely varies with mean annual temperature across biomes (Piao et al., 2010; Vanderwel et al., 2015). On the temporal scale, temperature-corrected respiration rates, as observed for stem



respiration of deciduous trees or for needle-leave evergreen trees, exhibit a seasonal variation leading to higher respiration rates during summer than during winter (Maier et al., 1998; Ceschia et al., 2002; Vose and Ryan, 2002; Zha et al., 2004).
290 Consistently, we observed a dampening of GPP_{vodtemp} during winter compared to GPP_{vod}. The addition of temperature thus seems to enable the model to reflect differences in basal respiration rates between growing and dormant periods in these regions. Although the temporal component of thermal acclimation of respiration appears to be the dominant contribution, the resulting dependency on temperature represents the cumulative effect of spatial and temporal thermal acclimation of respiration as the relationship for the temperature dependency was estimated from the data without a priori assumptions.

295 In addition to the temperature dependency, Ra also varies with tissue nitrogen content (Maier et al., 1998; Ceschia et al., 2002; Vose and Ryan, 2002; Tjoelker et al., 2008), which may thus contribute to uncertainties in the GPP estimation derived from VOD. Ra is also known to vary between plant tissues (Vose and Ryan, 2002; Gifford, 2003). The respiration of woody tissue is generally lower than for leaves (Vose and Ryan, 2002). Since VOD generally increases with the fraction of woody vegetation (Chaparro et al., 2019), using the median of VOD as model input may potentially compensate at least partly for
300 differences in respiration rates of stems and branches versus leaves within a grid cell.

4.2 Bias between GPP data sets

The addition of temperature dependency revealed contrasting results for the bias. While reductions in bias were observed for temperate and cold regions, a strong increase in bias was found for the tropics. Since the interaction term between VOD and T2M represents a 3D relationship, certain combinations of VOD and T2M intervals in the parameter space may not be
305 well represented by the training data. This may have caused the model to be not well constrained in certain regions, e.g. where temperature and VOD are very high, and thus might have contributed to the increase in bias in the tropics. Therefore, additional FLUXNET stations might help to better constrain the VOD-GPP model. Nevertheless, differences between the dataset were already evident at the site-level, which suggests that the observed difference at global scale may at least partly be caused by differences in the training dataset. In general, the agreement in annual GPP estimates is lowest in the tropics (Anav et al., 2015).
310 Estimates for the FLUXCOM RS setup, which was used in our study, were reported to yield lower global estimates than the FLUXCOM RS+METEO setup or GPP estimates from vegetation models (Jung et al., 2020). Similarly, MODIS was found to underestimate GPP in the tropics (Turner et al., 2006). The need for better constraints for GPP estimates especially in the tropics is well recognized (MacBean et al., 2018) and tackled in different studies (e.g., MacBean et al., 2018; Sun et al., 2018; Wu et al., 2020) but is usually hampered by the availability of in situ estimates.

315 4.3 The “zero-GPP problem” and non-structural carbohydrates

For GPP_{vodtemp}, we observed that winter GPP values for an example over Europe were slightly higher compared to GPP_{fluxcom} and GPP_{modis}. This issue of estimating GPP values close to zero was also observed in the scatter plots between GPP_{vodtemp} and in situ GPP_{fluxnet}. The reason for the overestimation at low GPP may be on the one hand an artefact related to the rehydration of plant residues after rain events and on the other hand may be explained by the sink-driven nature of our
320 approach. In the latter case, the non-zero GPP_{vodtemp} values may be caused by perennial vegetation. Both evergreen and de-



ciduous vegetation are respiring throughout the dormant period (Maier et al., 1998; Vose and Ryan, 2002) and concurrently are containing water. In turn, this presence of vegetation water content is detected through microwave sensors leading to non-zero GPPvodtemp estimates. It thus may point towards the existence of a storage term. In plants, photosynthetic assimilates can be stored in the form of non-structural carbohydrates (NSC), which can be converted back to plant usable sugars to support
325 respiration during the dormant period and growth at the start of the growing season (e.g., Martínez-Vilalta et al., 2016). For tropical forest plots, the balancing of plot level measurements of source and sink terms showed a decoupling between the two in response to drought which the authors attributed to the existence of NSC (Doughty et al., 2015). Therefore, such a storage term can thus support a temporary imbalance between sources and sinks of carbon, which may translate into differences between source- and sink-driven GPP.

330 4.4 Magnitude of input terms

Based on the partial dependency plots, we found that for the maintenance-related term, i.e. the interaction term between VOD and T2M, the value range is higher than for Δ VOD. Although our model represents the sum of NPP and growth Ra and not just growth Ra, the magnitude of the two input terms is consistent with studies that analyzed the contribution of maintenance and growth to Ra. For whole plants as well as for stem respiration of boreal needle-leave trees, maintenance respiration was shown
335 to play the dominant role for Ra with a contribution 70% (Chambers et al., 2004) and 80% (Zha et al., 2004), respectively.

4.5 Response to water availability

The analysis of VOD-GPP residuals with respect to FLUXCOM and MODIS revealed that GPPvodtemp largely showed a similar behavior as the independent GPP data sets as demonstrated by the widespread none significant correlations between with SPEI. This result is further supported by the general agreement in interannual variability. In addition to the possible impact
340 of NSC, occurrences of significant correlations between VOD-GPP residuals and SPEI may indicate different plant strategies for dealing with changes in dry or wet conditions. For negative correlations, this could be mainly related to differences in plant hydraulics, while for positive correlations, it might indicate shifts between above- and belowground carbon allocation.

Different plant strategies with regard to hydraulics can be expressed with the concept of isohydricity, which describes the regulation of stomatal control (Konings and Gentine, 2017; Giardina et al., 2018; Martínez-Vilalta and Garcia-Forner, 2017).
345 At ecosystem level, this parameter can be obtained using the difference in twice daily overpasses of microwave observations (Konings and Gentine, 2017). Although Martínez-Vilalta and Garcia-Forner (2017) argue that the regulation of water potential may not necessarily be strongly coupled with the assimilation during drought, the degree of isohydricity may still be an explanation for the observed variation in GPPvodtemp relative to GPPfluxcom and GPPmodis. Pronounced negative correlation for the analysis of GPP residuals were found in Argentina and the US corn belt, which are regions where Konings and Gentine
350 (2017) observed high values of isohydricity. Corn, which exhibits isohydric behavior (Lambers and Oliveira, 2019; Martínez-Vilalta and Garcia-Forner, 2017), i.e. is maintaining water potential through strong regulation of stomata, additionally has the ability, like other grasses, to roll up leaves in response to drought for reducing the loss of water from the plant's cuticular (e.g., Ribaut et al., 2009). In conjunction with the isohydric behavior, this might be an explanation for the strong signal reduction of



GPPfluxcom and GPPmodis relative to GPPvodtemp observed over Argentina. Although our analysis is based on 8-daily time
355 steps, characteristics of plant hydraulics which are retrieved from sub-daily data show similar features as for our analysis of
residuals between source- and sink-driven GPP in response to changes in water availability.

In contrast to the isohydric behavior, anisohydric behavior should not lead to pronounced differences between GPPvodtemp
and GPPfluxcom or GPPmodis as stomatal conductance and leaf water potential are both reduced in response to dry conditions
(Lambers and Oliveira, 2019). The anisohydric behavior thus potentially relates to the none significant correlations. Neverthe-
360 less, the degree of isohydricity may also vary between wet and dry season (Konings and Gentine, 2017), which also needs to
be taken into account for the interpretation of the residuals.

The observed positive correlations, i.e. reductions of GPPvodtemp relative to GPPfluxcom or GPPmodis, could be associated
with a stronger shift of assimilates to belowground plant organs. Different studies have shown that root growth may increase
in face of drought to maintain water access (Sanaullah et al., 2012; Burri et al., 2014) and consequently also nutrient supply
365 (Lambers and Oliveira, 2019). Since VOD observations only detect aboveground living vegetation, a shift towards belowground
plant organs may lead to apparently lower GPPvodtemp. Nevertheless, also the inverse, i.e. an increase of allocation to shoots,
was observed in the presence of legume species during drought (Sanaullah et al., 2012) and for tropical forest plots after
drought (Doughty et al., 2015).

Comparisons of GPPvodtemp with in situ observations of vegetation properties during such extreme events like drought,
370 however, may be needed to improve the understanding of the plant's response to changes in environmental conditions at the
ecosystem to global scale.

5 Conclusions

The VOD-GPP model was analyzed with regard to the impact of adding temperature as model input in order to account for
the temperature dependency of autotrophic respiration. The resulting GPP estimates, GPPvodtemp, showed a high consistency
375 with GPPfluxcom and GPPmodis for the temporal dynamic both at intra- and interannual time scale. For bias and error, the
addition of temperature resulted in a regionally diverse response with a general improvement for temperate and cold regions
and a decrease in performance mainly in the tropics. The improvement upon adding temperature, however, was less than might
have been expected, which indicates that the previous lack of temperature dependency in the model formulation can only
partly account for the observed differences between the global GPP datasets. Nevertheless, this result demonstrates that an
380 improvement by adding temperature is possible but might require further model constraints for a more robust estimation of
GPP.

The analysis of the VOD-GPP residuals revealed that GPPvodtemp largely yields a similar behavior as GPPfluxcom and
GPPmodis with respect to SPEI. This highlights that the relationship between VOD and GPP largely holds true even under
varying conditions of water availability. For some regions, where significant correlations were observed, the observed differ-
385 ences between GPPvodtemp and GPPfluxcom or GPPmodis may indicate different plant strategies for dealing with drought
conditions.



Overall, our results showed that GPPvodtemp potentially contains information on plant characteristics that may be relevant for large-scale ecological studies that are addressing the response to varying environmental conditions.

Data availability. VODCA products are available at <https://doi.org/10.5281/zenodo.2575599>. FLUXCOM products are available from <http://www.fluxcom.org> or on request to Martin Jung (mjung@bgc-jena.mpg.de). MODIS GPP estimates can be accessed at <https://lpdaac.usgs.gov/products/mod17a2hv006/>. Data from the FLUXNET network is available at <https://fluxnet.org/data/fluxnet2015-dataset/>.

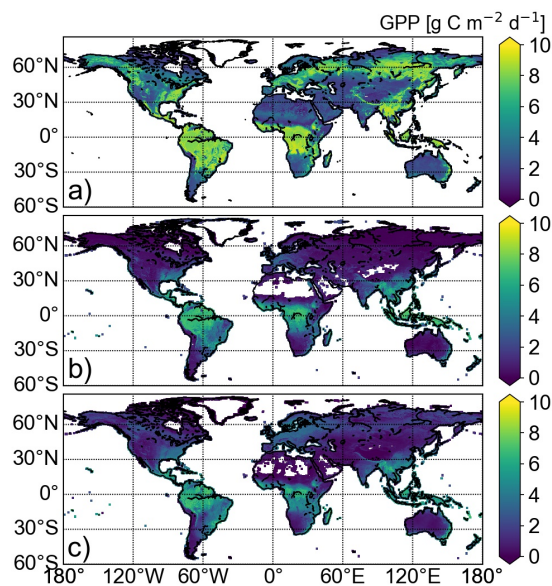


Figure A1. Temporal median maps for GPPvodtemp, GPPfluxcom and GPPmodis.

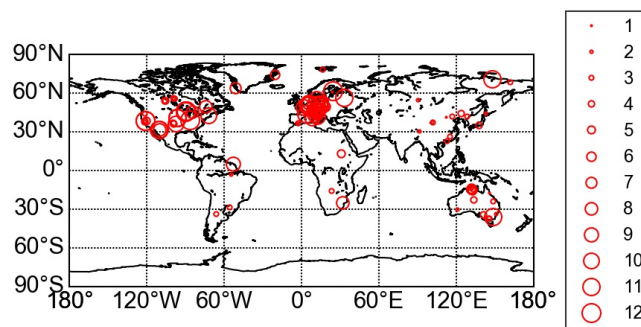


Figure A2. Location of FLUXNET Tier1 v1 stations within the period 2003 to 2014. The size of the circles represents the number of available station years.

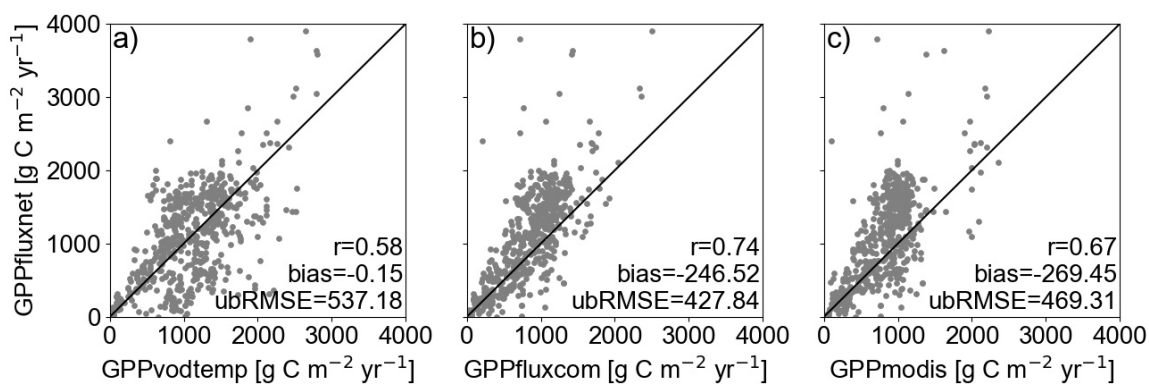


Figure A3. Scatterplot of annual GPP for GPPvodtemp, GPPfluxcom and GPPmodis versus GPPfluxnet.

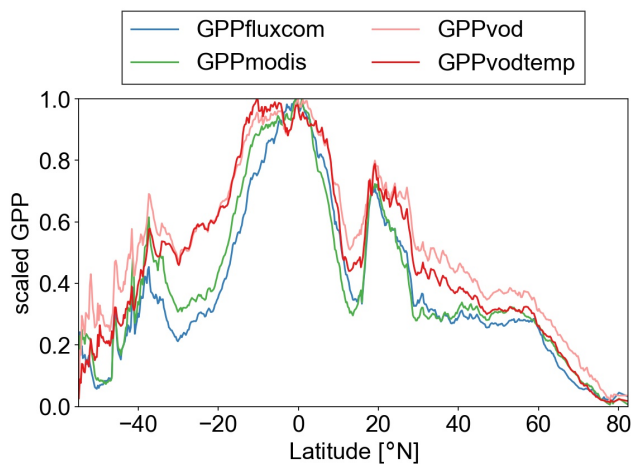


Figure A4. Scaled latitudinal distribution of annual GPP for GPPvodtemp, GPPvod, GPPfluxcom and GPPmodis. Data are computed relative to the latitudinal maximum for each data set.

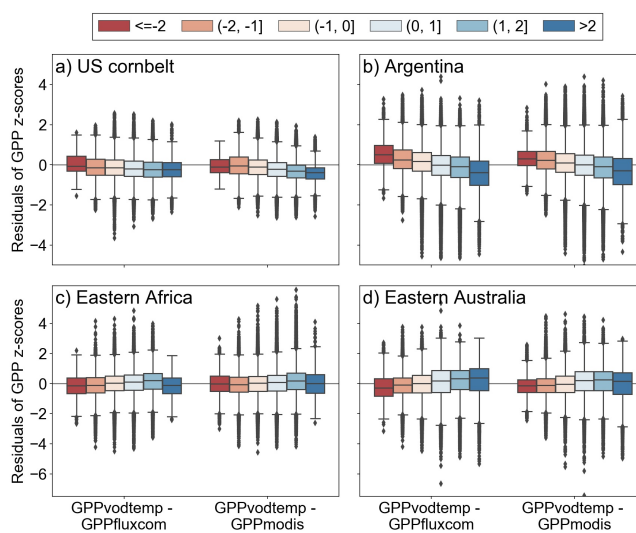


Figure A5. Boxplot of residuals between standardized GPP values of GPPvodtemp and GPPfluxcom or GPPmodis along SPEI12 categories for the data in Figure 8. The intervals for the different SPEI12 categories are given in the legend. Box whiskers indicate 1.5 of the interquartile range.



Table A1. Overview of FLUXNET Tier1 v1 stations within the analysis period 2003 to 2014.

FLUXNET-ID	name	lon	lat	years used
AR-SLu	San Luis	-66.46	-33.46	2009-2011
AR-Vir	Virasoro	-56.19	-28.24	2010-2012
AT-Neu	Neustift	11.32	47.12	2003-2012
AU-ASM	Alice Springs	133.25	-22.28	2010-2013
AU-Ade	Adelaide River	131.12	-13.08	2007-2009
AU-Cpr	Calperum	140.59	-34.00	2010-2013
AU-Cum	Cumberland Plains	150.72	-33.61	2012-2013
AU-DaP	Daly River Savanna	131.32	-14.06	2008-2013
AU-DaS	Daly River Cleared	131.39	-14.16	2008-2013
AU-Dry	Dry River	132.37	-15.26	2008-2013
AU-Emr	Emerald, Queensland, Australia	148.47	-23.86	2011-2013
AU-Fog	Fogg Dam	131.31	-12.55	2006-2008
AU-GWW	Great Western Woodlands, Western Australia, Australia	120.65	-30.19	2013-2014
AU-RDF	Red Dirt Melon Farm, Northern Territory	132.48	-14.56	2011-2013
AU-Rig	Riggs Creek	145.58	-36.65	2011-2013
AU-Rob	Robson Creek, Queensland, Australia	145.63	-17.12	2014-2014
AU-Tum	Tumbarumba	148.15	-35.66	2003-2013
AU-Whr	Whroo	145.03	-36.67	2011-2013
BE-Bra	Brasschaat	4.52	51.31	2004-2013
BE-Lon	Lonzee	4.75	50.55	2004-2014
BE-Vie	Vielsalm	6.00	50.31	2003-2014
BR-Sa3	Santarem-Km83-Logged Forest	-54.97	-3.02	2003-2004
CA-NS1	UCI-1850 burn site	-98.48	55.88	2003-2005
CA-NS3	UCI-1964 burn site	-98.38	55.91	2003-2005
CA-NS4	UCI-1964 burn site wet	-98.38	55.91	2003-2005
CA-NS5	UCI-1981 burn site	-98.49	55.86	2003-2005
CA-NS6	UCI-1989 burn site	-98.96	55.92	2003-2005
CA-NS7	UCI-1998 burn site	-99.95	56.64	2003-2005
CA-Qfo	Quebec - Eastern Boreal, Mature Black Spruce	-74.34	49.69	2003-2010
CA-SF1	Saskatchewan - Western Boreal, forest burned in 1977	-105.82	54.49	2003-2006
CA-SF2	Saskatchewan - Western Boreal, forest burned in 1989	-105.88	54.25	2003-2005
CA-SF3	Saskatchewan - Western Boreal, forest burned in 1998	-106.01	54.09	2003-2006
CH-Cha	Chamau	8.41	47.21	2006-2012

continued on next page



<i>continued from previous page</i>				
FLUXNET-ID	name	lon	lat	years used
CH-Fru	Früebüel	8.54	47.12	2006-2012
CH-Oe1	Oensingen grassland	7.73	47.29	2003-2008
CN-Cha	Changbaishan	128.10	42.40	2003-2005
CN-Cng	Changling	123.51	44.59	2007-2010
CN-Dan	Dangxiong	91.07	30.50	2004-2005
CN-Din	Dinghushan	112.54	23.17	2003-2005
CN-Du2	Duolun_grassland (D01)	116.28	42.05	2006-2008
CN-Ha2	Haibei Shrubland	101.33	37.61	2003-2005
CN-HaM	Haibei Alpine Tibet site	101.18	37.37	2003-2004
CN-Qia	Qianyanzhou	115.06	26.74	2003-2005
CN-Sw2	Siziwang Grazed (SZWG)	111.90	41.79	2010-2012
CZ-BK1	Bily Kriz forest	18.54	49.50	2003-2008
CZ-BK2	Bily Kriz grassland	18.54	49.49	2004-2006
DE-Akm	Anklam	13.68	53.87	2009-2014
DE-Gri	Grillenburg	13.51	50.95	2004-2014
DE-Hai	Hainich	10.45	51.08	2003-2012
DE-Kli	Klingenberg	13.52	50.89	2004-2014
DE-Lkb	Lackenberg	13.30	49.10	2009-2013
DE-Obe	Oberbärenburg	13.72	50.78	2008-2014
DE-RuS	Selhausen Juelich	6.45	50.87	2011-2014
DE-Spw	Spreewald	14.03	51.89	2010-2014
DE-Tha	Tharandt	13.57	50.96	2003-2014
DK-NuF	Nuuk Fen	-51.39	64.13	2008-2014
DK-Sor	Soroe	11.64	55.49	2003-2012
DK-ZaH	Zackenbergh Heath	-20.55	74.47	2003-2008
ES-LgS	Laguna Seca	-2.97	37.10	2007-2009
ES-Ln2	Lanjaron-Salvage logging	-3.48	36.97	2009-2009
FI-Hyy	Hyytiala	24.30	61.85	2003-2014
FI-Jok	Jokioinen	23.51	60.90	2003-2003
FR-Gri	Grignon	1.95	48.84	2004-2013
FR-Pue	Puechabon	3.60	43.74	2003-2013
GF-Guy	Guyafflux (French Guiana)	-52.92	5.28	2004-2012
IT-CA1	Castel d'Asso 1	12.03	42.38	2011-2013
IT-CA2	Castel d'Asso 2	12.03	42.38	2011-2013

continued on next page



<i>continued from previous page</i>				
FLUXNET-ID	name	lon	lat	years used
IT-CA3	Castel d' Asso 3	12.02	42.38	2011-2013
IT-Cp2	Castelporziano 2	12.36	41.70	2012-2013
IT-Isp	Ispira ABC-IS	8.63	45.81	2013-2014
IT-Lav	Lavarone	11.28	45.96	2003-2012
IT-Noe	Arca di Noé - Le Prigionette	8.15	40.61	2004-2012
IT-PT1	Parco Ticino forest	9.06	45.20	2003-2004
IT-Ren	Renon	11.43	46.59	2003-2013
IT-Ro1	Roccarespampani 1	11.93	42.41	2003-2008
IT-Ro2	Roccarespampani 2	11.92	42.39	2003-2012
IT-SR2	San Rossore 2	10.29	43.73	2013-2014
IT-SRo	San Rossore	10.28	43.73	2003-2012
IT-Tor	Torgnon	7.58	45.84	2008-2013
JP-MBF	Moshiri Birch Forest Site	142.32	44.39	2003-2005
JP-SMF	Seto Mixed Forest Site	137.08	35.26	2003-2006
NL-Hor	Horstermeer	5.07	52.24	2004-2011
NL-Loo	Loobos	5.74	52.17	2003-2013
NO-Adv	Adventdalen	15.92	78.19	2012-2014
RU-Che	Cherski	161.34	68.61	2003-2005
RU-Cok	Chokurdakh	147.49	70.83	2003-2013
RU-Fyo	Fyodorovskoye	32.92	56.46	2003-2013
RU-Ha1	Hakasia steppe	90.00	54.73	2003-2004
SD-Dem	Demokeya	30.48	13.28	2005-2009
US-AR1	ARM USDA UNL OSU Woodward Switchgrass 1	-99.42	36.43	2009-2012
US-AR2	ARM USDA UNL OSU Woodward Switchgrass 2	-99.60	36.64	2009-2012
US-ARM	ARM Southern Great Plains site- Lamont	-97.49	36.61	2003-2012
US-Blo	Blodgett Forest	-120.63	38.90	2003-2007
US-Ha1	Harvard Forest EMS Tower (HFR1)	-72.17	42.54	2003-2012
US-Los	Lost Creek	-89.98	46.08	2003-2014
US-MMS	Morgan Monroe State Forest	-86.41	39.32	2003-2014
US-Me6	Metolius Young Pine Burn	-121.61	44.32	2010-2012
US-Myb	Mayberry Wetland	-121.77	38.05	2011-2014
US-Ne1	Mead - irrigated continuous maize site	-96.48	41.17	2003-2013
US-Ne2	Mead - irrigated maize-soybean rotation site	-96.47	41.16	2003-2013
US-Ne3	Mead - rainfed maize-soybean rotation site	-96.44	41.18	2003-2013

continued on next page



<i>continued from previous page</i>				
FLUXNET-ID	name	lon	lat	years used
US-SRM	Santa Rita Mesquite	-110.87	31.82	2004-2014
US-Syv	Sylvania Wilderness Area	-89.35	46.24	2003-2014
US-Ton	Tonzi Ranch	-120.97	38.43	2003-2014
US-Tw3	Twitchell Alfalfa	-121.65	38.12	2013-2014
US-UMd	UMBS Disturbance	-84.70	45.56	2007-2014
US-Var	Vaira Ranch- Ione	-120.95	38.41	2003-2014
US-WCr	Willow Creek	-90.08	45.81	2003-2014
US-Whs	Walnut Gulch Lucky Hills Shrub	-110.05	31.74	2007-2014
US-Wkg	Walnut Gulch Kendall Grasslands	-109.94	31.74	2004-2014
ZA-Kru	Skukuza	31.50	-25.02	2003-2010
ZM-Mon	Mongu	23.25	-15.44	2007-2009

Author contributions. IT conceived the study, carried out the analysis and drafted the manuscript with contributions from WD and MF on the study design. BW contributed to data preparation. LM provided VOD estimates from VODCA. All authors discussed the results and commented on the manuscript.

Competing interests. The authors declare that they have no conflict of interest.

Acknowledgements. Wouter Dorigo and Benjamin Wild are supported through the EOWAVE project funded by the TU Wien Wissenschaftspreis 2015, which was awarded to Wouter Dorigo (<http://climners.geo.tuwien.ac.at/eowave/>). This work used eddy covariance data acquired and shared by the FLUXNET community, including these networks: AmeriFlux, AfriFlux, AsiaFlux, CarboAfrica, CarboEuropeIP, CarboItaly, CarboMont, ChinaFlux, Fluxnet-Canada, GreenGrass, ICOS, KoFlux, LBA, NECC, OzFlux-TERN, TCOS-Siberia, and USCCC. The FLUXNET eddy covariance data processing and harmonization was carried out by the ICOS Ecosystem Thematic Center, AmeriFlux Management Project and Fluxdata project of FLUXNET, with the support of CDIAC, and the OzFlux, ChinaFlux and AsiaFlux offices.



References

- Anav, A., Friedlingstein, P., Beer, C., Ciais, P., Harper, A., Jones, C., Murray-Tortarolo, G., Papale, D., Parazoo, N. C., Peylin, P., et al.:
410 Spatiotemporal patterns of terrestrial gross primary production: A review, *Reviews of Geophysics*, 53, 785–818, 2015.
- Atkin, O. K. and Tjoelker, M. G.: Thermal acclimation and the dynamic response of plant respiration to temperature, *Trends in plant science*,
8, 343–351, 2003.
- Atkin, O. K., Atkinson, L. J., Fisher, R. A., Campbell, C. D., ZARAGOZA-CASTELLS, J., Pitchford, J. W., Woodward, F. I., and Hurry,
V.: Using temperature-dependent changes in leaf scaling relationships to quantitatively account for thermal acclimation of respiration in a
415 coupled global climate–vegetation model, *Global change biology*, 14, 2709–2726, 2008.
- Beguiría, S., Latorre, B., Reig, F., and Vicente-Serrano, S.: sbeguiria/SPEIbase: Version 2.5. 1, Glob. SPEI Database, 2017.
- Burri, S., Sturm, P., Prechsl, U. E., Knohl, A., and Buchmann, N.: The impact of extreme summer drought on the short-term carbon coupling
of photosynthesis to soil CO₂ efflux in a temperate grassland, *Biogeosciences*, 11, 961–975, 2014.
- C3S: C3S ERA5-Land reanalysis. Copernicus Climate Change Service, <https://cds.climate.copernicus.eu/cdsapp#!/home>, 15.11.2019, 2019.
- 420 Ceschia, É., Damesin, C., Lebaube, S., Pontailier, J.-Y., and Dufrière, É.: Spatial and seasonal variations in stem respiration of beech trees
(*Fagus sylvatica*), *Annals of Forest Science*, 59, 801–812, 2002.
- Chambers, J. Q., Tribuzy, E. S., Toledo, L. C., Crispim, B. F., Higuchi, N., Santos, J. d., Araújo, A. C., Kruijt, B., Nobre, A. D., and Trumbore,
S. E.: Respiration from a tropical forest ecosystem: partitioning of sources and low carbon use efficiency, *Ecological Applications*, 14,
72–88, 2004.
- 425 Chaparro, D., Duveiller, G., Piles, M., Cescatti, A., Vall-Llossera, M., Camps, A., and Entekhabi, D.: Sensitivity of L-band vegetation optical
depth to carbon stocks in tropical forests: a comparison to higher frequencies and optical indices, *Remote sensing of environment*, 232,
111 303, 2019.
- Crocetti, L., Forkel, M., Fischer, M., Jurečka, F., Grlj, A., Salentinig, A., Trnka, M., Anderson, M., Ng, W.-T., Kokalj, Ž., et al.: Earth
Observation for agricultural drought monitoring in the Pannonian Basin (southeastern Europe): current state and future directions, *Regional
430 Environmental Change*, 20, 1–17, 2020.
- Doughty, C. E., Metcalfe, D., Girardin, C. A., Amezquita, F. F., Durand, L., Huasco, W. H., Silva-Espejo, J. E., Araujo-Murakami, A.,
Da Costa, M., da Costa, A. C. L., et al.: Source and sink carbon dynamics and carbon allocation in the Amazon basin, *Global Biogeo-
chemical Cycles*, 29, 645–655, 2015.
- El Hajj, M., Baghdadi, N., Wigneron, J.-P., Zribi, M., Albergel, C., Calvet, J.-C., and Fayad, I.: First Vegetation Optical Depth Mapping from
435 Sentinel-1 C-band SAR Data over Crop Fields, *Remote Sensing*, 11, 2769, 2019.
- Forkel, M., Dorigo, W., Lasslop, G., Chuvieco, E., Hantson, S., Heil, A., Teubner, I., Thonicke, K., and Harrison, S. P.: Recent global and
regional trends in burned area and their compensating environmental controls, *Environmental Research Communications*, 1, 051 005,
2019.
- Giardina, F., Konings, A. G., Kennedy, D., Alemohammad, S. H., Oliveira, R. S., Uriarte, M., and Gentine, P.: Tall Amazonian forests are
440 less sensitive to precipitation variability, *Nature Geoscience*, 11, 405–409, 2018.
- Gifford, R. M.: Plant respiration in productivity models: conceptualisation, representation and issues for global terrestrial carbon-cycle
research, *Functional Plant Biology*, 30, 171–186, 2003.
- Gilberto, P., Trotta, C., Eleonora, C., Housen, C., Christianson, D., You-Wei, C., Poindexter, C., Chen, J., Abdelrahman, E., Humphrey, M.,
et al.: The FLUXNET2015 dataset and the ONEFlux processing pipeline for eddy covariance data, *Scientific Data*, 7, 2020.



- 445 Goodrich, J., Campbell, D., Clearwater, M., Rutledge, S., and Schipper, L.: High vapor pressure deficit constrains GPP and the light response of NEE at a Southern Hemisphere bog, *Agricultural and Forest Meteorology*, 203, 54–63, 2015.
- Hastie, T. and Tibshirani, R.: Generalized additive models: some applications, *Journal of the American Statistical Association*, 82, 371–386, 1987.
- Hersbach, H., Bell, B., Berrisford, P., Hirahara, S., Horányi, A., Muñoz-Sabater, J., Nicolas, J., Peubey, C., Radu, R., Schepers, D., et al.:
450 The ERA5 global reanalysis, *Quarterly Journal of the Royal Meteorological Society*, 146, 1999–2049, 2020.
- Jung, M., Schwalm, C., Migliavacca, M., Walther, S., Camps-Valls, G., Koirala, S., Anthoni, P., Besnard, S., Bodesheim, P., Carvalhais, N., et al.: Scaling carbon fluxes from eddy covariance sites to globe: synthesis and evaluation of the FLUXCOM approach, *Biogeosciences*, 17, 1343–1365, 2020.
- Konings, A. G. and Gentine, P.: Global variations in ecosystem-scale isohydricity, *Global change biology*, 23, 891–905, 2017.
- 455 Konings, A. G., Rao, K., and Steele-Dunne, S. C.: Macro to micro: microwave remote sensing of plant water content for physiology and ecology, *New Phytologist*, 223, 1166–1172, 2019.
- Kumar, S. V., Holmes, T. R., Bindlish, R., Jeu, R. d., and Peters-Lidard, C.: Assimilation of vegetation optical depth retrievals from passive microwave radiometry, *Hydrology and Earth System Sciences*, 24, 3431–3450, 2020.
- Lambers, H. and Oliveira, R. S.: Plant water relations, in: *Plant physiological ecology*, pp. 187–263, Springer, 2019.
- 460 Li, L., Njoku, E. G., Im, E., Chang, P. S., and Germain, K. S.: A preliminary survey of radio-frequency interference over the US in Aqua AMSR-E data, *IEEE Transactions on Geoscience and Remote Sensing*, 42, 380–390, 2004.
- Liu, Y. Y., Van Dijk, A. I., De Jeu, R. A., Canadell, J. G., McCabe, M. F., Evans, J. P., and Wang, G.: Recent reversal in loss of global terrestrial biomass, *Nature Climate Change*, 5, 470–474, 2015.
- MacBean, N., Maignan, F., Bacour, C., Lewis, P., Peylin, P., Guanter, L., Köhler, P., Gómez-Dans, J., and Disney, M.: Strong constraint on
465 modelled global carbon uptake using solar-induced chlorophyll fluorescence data, *Scientific reports*, 8, 1973, 2018.
- Maier, C. A., Zarnoch, S. J., and Dougherty, P.: Effects of temperature and tissue nitrogen on dormant season stem and branch maintenance respiration in a young loblolly pine (*Pinus taeda*) plantation, *Tree Physiology*, 18, 11–20, 1998.
- Martínez-Vilalta, J. and Garcia-Forner, N.: Water potential regulation, stomatal behaviour and hydraulic transport under drought: deconstructing the iso/anisohydric concept, *Plant, Cell & Environment*, 40, 962–976, 2017.
- 470 Martínez-Vilalta, J., Sala, A., Asensio, D., Galiano, L., Hoch, G., Palacio, S., Piper, F. I., and Lloret, F.: Dynamics of non-structural carbohydrates in terrestrial plants: a global synthesis, *Ecological Monographs*, 86, 495–516, 2016.
- Moesinger, L., Dorigo, W., de Jeu, R., van der Schalie, R., Scanlon, T., Teubner, I., and Forkel, M.: The global long-term microwave Vegetation Optical Depth Climate Archive (VODCA), *Earth System Science Data*, 12, 177–196, 2020.
- Momen, M., Wood, J. D., Novick, K. A., Pangle, R., Pockman, W. T., McDowell, N. G., and Konings, A. G.: Interacting effects of leaf water
475 potential and biomass on vegetation optical depth, *Journal of Geophysical Research: Biogeosciences*, 122, 3031–3046, 2017.
- Monteith, J.: Solar radiation and productivity in tropical ecosystems, *Journal of applied ecology*, 9, 747–766, 1972.
- Muñoz-Sabater, J.: First ERA5-Land dataset to be released this spring, ECMWF: Reding, UK, 2019.
- Njoku, E. G., Ashcroft, P., Chan, T. K., and Li, L.: Global survey and statistics of radio-frequency interference in AMSR-E land observations, *IEEE Transactions on Geoscience and Remote Sensing*, 43, 938–947, 2005.
- 480 Piao, S., Luysaert, S., Ciais, P., Janssens, I. A., Chen, A., Cao, C., Fang, J., Friedlingstein, P., Luo, Y., and Wang, S.: Forest annual carbon cost: A global-scale analysis of autotrophic respiration, *Ecology*, 91, 652–661, 2010.



- Rao, K., Anderegg, W. R., Sala, A., Martínez-Vilalta, J., and Konings, A. G.: Satellite-based vegetation optical depth as an indicator of drought-driven tree mortality, *Remote Sensing of Environment*, 227, 125–136, 2019.
- Ribaut, J.-M., Betran, J., Monneveux, P., and Setter, T.: Drought tolerance in maize, in: *Handbook of maize: its biology*, pp. 311–344, 485 Springer, 2009.
- Running, S., Mu, Q., and Zhao, M.: MOD17A2H MODIS/terra gross primary productivity 8-day L4 global 500m SIN grid V006, NASA EOSDIS Land Processes DAAC, 2015.
- Running, S. W., Nemani, R., Glassy, J. M., and Thornton, P. E.: MODIS daily photosynthesis (PSN) and annual net primary production (NPP) product (MOD17) Algorithm Theoretical Basis Document, University of Montana, SCF At-Launch Algorithm ATBD Documents 490 (available online at: www.nts.gov/umt.edu/modis/ATBD/ATBD_MOD17_v21.pdf), 1999.
- Running, S. W., Thornton, P. E., Nemani, R., and Glassy, J. M.: Global terrestrial gross and net primary productivity from the earth observing system, in: *Methods in ecosystem science*, pp. 44–57, Springer, 2000.
- Running, S. W., Nemani, R. R., Heinsch, F. A., Zhao, M., Reeves, M., and Hashimoto, H.: A continuous satellite-derived measure of global terrestrial primary production, *Bioscience*, 54, 547–560, 2004.
- 495 Ryan, M. G., Lavigne, M. B., and Gower, S. T.: Annual carbon cost of autotrophic respiration in boreal forest ecosystems in relation to species and climate, *Journal of Geophysical Research: Atmospheres*, 102, 28 871–28 883, 1997.
- Sanaullah, M., Chabbi, A., Rumpel, C., and Kuzyakov, Y.: Carbon allocation in grassland communities under drought stress followed by 14C pulse labeling, *Soil Biology and Biochemistry*, 55, 132–139, 2012.
- Sapes, G., Roskill, B., Dobrowski, S., Maneta, M., Anderegg, W. R., Martínez-Vilalta, J., and Sala, A.: Plant water content integrates 500 hydraulics and carbon depletion to predict drought-induced seedling mortality, *Tree physiology*, 39, 1300–1312, 2019.
- Servén, D. and Brummitt, C.: pyGAM: generalized additive models in python, Zenodo. DOI, 10, <https://doi.org/http://doi.org/10.5281/zenodo.1208723>, 2018.
- Smith, N. G. and Dukes, J. S.: Plant respiration and photosynthesis in global-scale models: incorporating acclimation to temperature and CO₂, *Global change biology*, 19, 45–63, 2013.
- 505 Song, L., Li, Y., Ren, Y., Wu, X., Guo, B., Tang, X., Shi, W., Ma, M., Han, X., and Zhao, L.: Divergent vegetation responses to extreme spring and summer droughts in Southwestern China, *Agricultural and Forest Meteorology*, 279, 107 703, 2019.
- Sun, Y., Frankenberg, C., Jung, M., Joiner, J., Guanter, L., Köhler, P., and Magney, T.: Overview of Solar-Induced chlorophyll Fluorescence (SIF) from the Orbiting Carbon Observatory-2: Retrieval, cross-mission comparison, and global monitoring for GPP, *Remote Sensing of Environment*, 209, 808–823, 2018.
- 510 Teubner, I. E., Forkel, M., Jung, M., Liu, Y. Y., Miralles, D. G., Parinussa, R., van der Schalie, R., Vreugdenhil, M., Schwalm, C. R., Tramontana, G., et al.: Assessing the relationship between microwave vegetation optical depth and gross primary production, *International journal of applied earth observation and geoinformation*, 65, 79–91, 2018.
- Teubner, I. E., Forkel, M., Camps-Valls, G., Jung, M., Miralles, D. G., Tramontana, G., van der Schalie, R., Vreugdenhil, M., Möisinger, L., and Dorigo, W. A.: A carbon sink-driven approach to estimate gross primary production from microwave satellite observations, *Remote 515 Sensing of Environment*, 229, 100–113, 2019.
- Tjoelker, M. G., Oleksyn, J., and Reich, P. B.: Modelling respiration of vegetation: evidence for a general temperature-dependent Q₁₀, *Global Change Biology*, 7, 223–230, 2001.
- Tjoelker, M. G., Oleksyn, J., Reich, P. B., and Żytkowiak, R.: Coupling of respiration, nitrogen, and sugars underlies convergent temperature acclimation in *Pinus banksiana* across wide-ranging sites and populations, *Global Change Biology*, 14, 782–797, 2008.



- 520 Turner, D. P., Ritts, W. D., Cohen, W. B., Maersperger, T. K., Gower, S. T., Kirschbaum, A. A., Running, S. W., Zhao, M., Wofsy, S. C., Dunn, A. L., et al.: Site-level evaluation of satellite-based global terrestrial gross primary production and net primary production monitoring, *Global Change Biology*, 11, 666–684, 2005.
- Turner, D. P., Ritts, W. D., Cohen, W. B., Gower, S. T., Running, S. W., Zhao, M., Costa, M. H., Kirschbaum, A. A., Ham, J. M., Saleska, S. R., et al.: Evaluation of MODIS NPP and GPP products across multiple biomes, *Remote sensing of environment*, 102, 282–292, 2006.
- 525 van der Schalie, R., de Jeu, R. A., Kerr, Y., Wigneron, J.-P., Rodríguez-Fernández, N. J., Al-Yaari, A., Parinussa, R. M., Mecklenburg, S., and Drusch, M.: The merging of radiative transfer based surface soil moisture data from SMOS and AMSR-E, *Remote Sensing of Environment*, 189, 180–193, 2017.
- Vanderwel, M. C., Slot, M., Lichstein, J. W., Reich, P. B., Kattge, J., Atkin, O. K., Bloomfield, K. J., Tjoelker, M. G., and Kitajima, K.: Global convergence in leaf respiration from estimates of thermal acclimation across time and space, *New Phytologist*, 207, 1026–1037, 2015.
- 530 Vicente-Serrano, S. M., Beguería, S., López-Moreno, J. I., Angulo, M., and El Kenawy, A.: A new global 0.5 gridded dataset (1901–2006) of a multiscalar drought index: comparison with current drought index datasets based on the Palmer Drought Severity Index, *Journal of Hydrometeorology*, 11, 1033–1043, 2010.
- Vose, J. M. and Ryan, M. G.: Seasonal respiration of foliage, fine roots, and woody tissues in relation to growth, tissue N, and photosynthesis, *Global Change Biology*, 8, 182–193, 2002.
- 535 Vreugdenhil, M., Wagner, W., Bauer-Marschallinger, B., Pfeil, I., Teubner, I., Rüdiger, C., and Strauss, P.: Sensitivity of Sentinel-1 backscatter to vegetation dynamics: An Austrian case study, *Remote Sensing*, 10, 1396, 2018.
- Wu, M., Scholze, M., Kaminski, T., Voßbeck, M., and Tagesson, T.: Using SMOS soil moisture data combining CO₂ flask samples to constrain carbon fluxes during 2010–2015 within a Carbon Cycle Data Assimilation System (CCDAS), *Remote Sensing of Environment*, 240, 111 719, 2020.
- 540 Wythers, K. R., Reich, P. B., and Bradford, J. B.: Incorporating temperature-sensitive Q₁₀ and foliar respiration acclimation algorithms modifies modeled ecosystem responses to global change, *Journal of Geophysical Research: Biogeosciences*, 118, 77–90, 2013.
- Zha, T., Kellomäki, S., Wang, K.-Y., Ryyppö, A., and Niinistö, S.: Seasonal and annual stem respiration of Scots pine trees under boreal conditions, *Annals of Botany*, 94, 889–896, 2004.
- 545 Zhang, Y., Xiao, X., Zhou, S., Ciais, P., McCarthy, H., and Luo, Y.: Canopy and physiological controls of GPP during drought and heat wave, *Geophysical Research Letters*, 43, 3325–3333, 2016.
- Zhang, Y., Xiao, X., Wu, X., Zhou, S., Zhang, G., Qin, Y., and Dong, J.: A global moderate resolution dataset of gross primary production of vegetation for 2000–2016, *Scientific data*, 4, 170 165, 2017.
- Zhang, Y., Zhou, S., Gentine, P., and Xiao, X.: Can vegetation optical depth reflect changes in leaf water potential during soil moisture dry-down events?, *Remote Sensing of Environment*, 234, 111 451, 2019.
- 550